Characterizing Potential Surface Topographies through the Distribution of Saddles and Minima

Graham Cox and R. Stephen Berry*

Department of Chemistry and The James Franck Institute, The University of Chicago, 5735 South Ellis Avenue, Chicago Illinois 60637-1403

Roy L. Johnston

School of Chemistry, The University of Birmingham, Birmingham, England, B15 2TT

Received: May 18, 2006; In Final Form: August 4, 2006

Three related clusters of thirteen particles bound by pairwise Morse potentials with different ranges are the vehicles for relating the dynamics and kinetics of these clusters to the topographies of their energy landscapes. The analyses are based on the distributions of minima and saddles, on the asymmetries of the barriers and the kinetics of passage among the energy bands that the distributions of minima display. While all three of the examples are essentially structure-seekers, the extent of this character is clearly related to the range of the potential.

1. Introduction

Clusters represent an important area of material science, bridging the gap between atomic and bulk behavior.[1] There have been many studies undertaken to investigate the dynamics of potential energy surfaces of clusters, using master equations on statistical samples,[2] interbasin dynamics,[3] scalefree topologies of inherent structure networks (ISN),[4] and discrete path sampling (DPS),[5] to mention a few.

This study, however, focuses on characterizing how features of the topography of the system's energy landscape govern its behavior. Specifically, we examine how the degree of local asymmetry of a surface reflects and indicates the extent to which a system is "structure-seeking" (i.e., in the extreme case, this relates to a surface which is focused/funneled toward the global minimum) or is "glass-forming" (i.e., a rugged surface with no funneling toward low-lying minima). Previous studies[6,10] have shown at least qualitatively, through analysis of linked minima and saddles, that systems with sawtooth potential surface topographies are good glass-formers, whereas those with staircase-like topographies are good structure-seekers.[7] The surface topologies of 6-, 7-, and 13-atom clusters bound by pairwise Morse potentials[8] have been analyzed for several values of the dimensionless range parameter ρ.[9,10] (The value $\rho = 6$ simulates argon.) A database (DB) of transitions has been obtained for ρ values of 3, 4, 5, and 6 using the method of eigenvector following.[18] These databases are thought to be nearly complete (for $\rho = 5$ and 6, a small high-energy basin is not connected to the main basin, showing that at least one high-energy saddle between them has not been found), mapping out the minima and saddles of the respective potential surfaces.

For many values of ρ, a 13-atom Morse cluster (M_{13}) constitutes a magic number cluster: those investigated here have icosahedral global minima,[11] with a potential surface composed of a single basin. By "basin," we mean the region including a deep minimum on the potential surface and the parts of the landscape that lead down to it either directly or by sequences of minima and saddles whose minima drop monotonically in energy as they approach that stable lowest minimum, the basin bottom. It is certainly possible to invent topographies in which there might be ambiguity about what constitutes a "basin," but these seem to be rare enough to allow us to disregard them and use the term generally here. Studies have focused on the structural consequences of the value of the Morse range parameter.[9,12] The M_{13} ($\rho = 6$) global minimum is easily found in molecular dynamic simulations, and this cluster is considered a good structure-seeker. This is in contrast to some larger Lennard-Jones and Morse clusters, which are good examples of glass-formers.[6] The ρ parameter of the Morse potential varies the potential's range: the smaller the value of ρ, the longer the range of the potential. Morse potentials fit to known diatomic molecule spectra have values of ρ between 3 and 7. Long-range potentials yield smoother surfaces than short-range, with small atomic rearrangements of distant atoms buffering the effect of larger structural local rearrangements and with significant many-body contributions to most well-to-well rearrangements. The effect of longer-range interactions is to lower barrier heights, providing better structure-seeker topographies. A large ρ value, i.e., a short-range potential, gives rise to a rougher surface, with larger barriers, and hence to a more sawtooth-like topography. Although the ρ values studied here for M_{13} all correspond to structure-seekers to different degrees, increasing ρ clearly slides the topography along the scale from structure-seeking toward glass-forming. Wales has shown how the effects of the value of the range of interparticle potential on the topography, especially the stationary points of the surface, can be interpreted in terms of catastrophe theory.[13] In particular, the behavior, especially the appearance or disappearance, of zeros of the Hessian of the surface can be related to the appearance of specific kinds of "catastrophes" such as the fold catastrophe in which a high minimum and the saddle that separates it from a deeper minimum converge to a single stationary point.

One point, basically one of semantics, must be introduced here. The term "structure-seeker" was introduced to describe systems that, except under very extreme quenching conditions,

10.1021/jp0630572 CCC: $33.50 © 2006 American Chemical Society
Published on Web 09/19/2006

find their way, typically during a cooling process but also implicitly in any relaxation process, to a very small, low-lying subset of stationary states on the potential energy landscape. The term "glass-former" was introduced to describe systems that cool or otherwise relax to something approaching a statistical distribution of all the accessible local minima.[6,7] The idea that "structure-seeker" might mean "able to find the global minimum" was not in any way intended, and in fact, the contexts in which these concepts were first used were those of systems with landscapes having several deep, very stable minima. One could of course use the term "structure-seeker" for a system with a single deep minimum, as is generally presumed for most globular proteins, but it is only because of that specific form of topography, with a single dominant basin, that the term would imply that the system would find only a single minimum. In fact, one would surely want to call a prion a "structure-seeker" regardless of whether the prion state is the global minimum. In short, "structure-seeker" means "able to relax to one of a set of structures very small compared with the set of all local minima", and "glass-former" means "relaxes to any of a very large fraction of the available local minima". In the context of the catastrophe analysis,[13] the systems considered glass-formers have an exponentially large number of accessible local minima, which is certainly consistent with the usage here.

The main goals of this study are (a) to investigate quantitatively how variation of the range of the interparticle potential affects the degree to which a system is an effective structure-seeker insofar as it affects the topography of the potential, and (b) to examine especially the way the heights and asymmetries of the saddles between minima affect the natural motions of the system on its potential surface, especially with respect to its structure-seeking tendencies. In this sense, the focus here, being on relations between topography and dynamics, is complementary to the correlations that have been studied previously between different aspects of the topography of the potential landscape; see, for example, the study by Wales and Doye.[14]

2. Minima and Saddles

Previous studies have shown the frequency distribution for minima with respect to energy for $\rho = 4$, 6, 10, and 14.[15] Therefore, in this study, we only show this distribution for $\rho = 5$ (Figure 1a), including the frequency distribution of the saddles. For all values of ρ, there is a large energy gap between the global and secondary local minima. This is most apparent in the respective disconnectivity graphs.[15,16] The standard disconnectivity graph for $\rho = 5$ is shown in Figure 1b.

This representation of topography, when applied to simple proteins, indicates their ability to fold, particularly to show why they fold reliably to their native structures. (A complementary approach to such interpretations that gives a finer-grained view at the cost of somewhat greater data analysis is the use of monotonic sequences of stationary points.[6,17]) The deep well of the global minimum gives Ar_{13} as a distinct solid phase, with an icosahedral global minimum.

The distributions of both minima and saddles, with respect to energy, are skewed toward higher energy. The distributions of minima show clear, distinct bands corresponding to preferred energy ranges, mirrored closely by similar bands in the saddle distributions, which, as one would expect, are shifted slightly to energies higher than those of the minima. As the potential range shortens, the bandwidths of the distributions become smaller. This reflects how a cluster which is bound by shorter-range forces is less able to buffer against the energy requirements for local structural rearrangements by making small movements of distant atoms (i.e., cooperative rearrangements.[23] A shorter-ranged interaction potential, giving rise to a lower degree of cooperative motion, distributes the minima into more distinct bands. With a more discretized distribution of minima, the relaxation becomes more difficult: the system finds no guiding pathway to a selected minimum and, instead, tends to make transitions between minima with comparable energies.

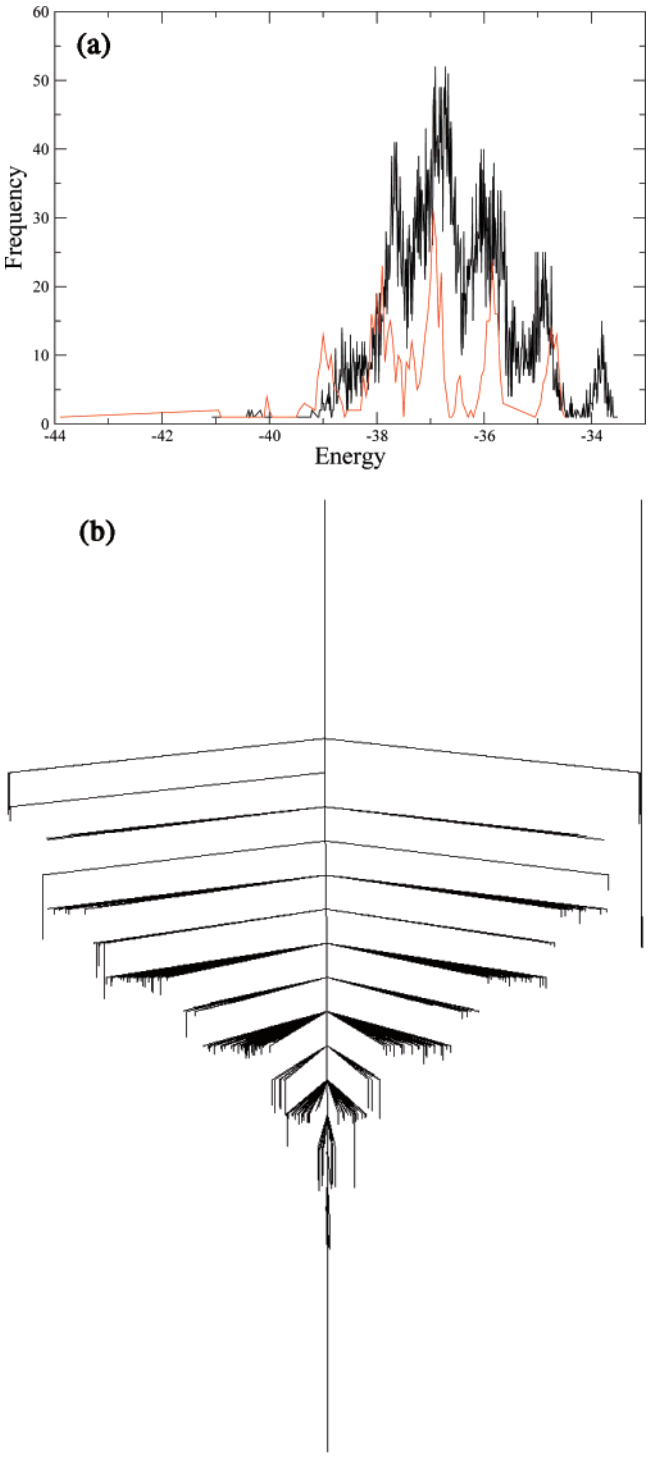

Figure 1. For the M_{13} cluster with $\rho = 5$: (a) frequency distribution of energies of minima (red) and saddles (black); (b) disconnectivity graph with energy ranging from a maximum of -30.00 to the global minimum at -43.95.

We now make the following definitions:

1. E_l − the lower-energy minimum in a transition.

TABLE 1: Linear Regression Correlation Coefficients Varying ρ for M_9 and M_{13}

linear regression correlation of ...	M_9 coefficients for ρ = 3	4	5	6	M_{13} coefficients for ρ = 3	4	5	6
B_l vs M_d	0.996	0.527	0.757	0.747	0.957	0.834	0.875	0.874
B_h vs M_d	0.073	0.023	0.167	0.187	0.327	0.134	0.104	0.062
D_{cs} vs I_{pl}	0.780	0.706	0.734	0.520	0.856	0.784	0.700	0.579
B_l vs D_{cs}	0.835	0.910	0.816	0.736	0.872	0.795	0.780	0.724
B_l vs I_{pl}	0.894	0.698	0.560	0.267	0.758	0.734	0.653	0.550
M_d vs D_{cs}	0.789	0.307	0.337	0.265	0.771	0.546	0.580	0.502
M_d vs I_{pl}	0.883	0.076	0.280	0.020	0.695	0.386	0.416	0.382

2. E_h − the higher-energy minimum in a transition.

3. B_l − the energy barrier between the lower minimum and the saddle.

4. B_h − the energy barrier between the higher minimum and the saddle.

5. M_d − the energy difference between a pair of minima.

6. D_{cs} − the distance in coordinate space between a pair of minima.

7. I_{pl} − the integrated path length between a pair of minima.

A previous study[18] looked at correlations using linear regression on clusters of 55 atoms and 55 C_{60} molecules bound by Lennard-Jones forces (LJ_{55}). Here, the analysis is extended to include correlations for the Ar_9 and Ar_{13} clusters, shown in Table 1. (This study did not include the very high value, 13.6, used for the cluster of C_{60} molecules: that system seems to be the shortest-range molecular system known.)

From Table 1, we draw the following observations:

1. The higher the B_l, the greater the M_d. With the exception of $\rho = 4$, as the potential range is reduced, the correlation decreases. The high correlation observed for all values of ρ indicates that all these surfaces are structure-seeking, albeit to different degrees.

2. There is no significant correlation (above 0.5) between B_h and M_d for any potential range. This indicates a number of favorable relaxation paths to different lower-energy minima that are indistinguishable by barrier height alone.

3. The longer the I_{pl} between a pair of minima, the larger their D_{cs}. This correlation holds, however, to a lesser extent than in a previous study by Wales:[18] for LJ_{55}, the correlation is 0.89, and for $(C_{60})_{55}$, it is 0.93. Again, the correlation drops off for shorter-ranged potentials.

4. The higher the B_l, the greater the D_{cs} and I_{pl} between minima. The strong D_{cs} correlations suggest that a cluster undergoes significant structural rearrangement as it descends from a saddle to E_l. Weaker values of this correlation suggest that the surface is rougher, implying that a small structural change can produce a large difference in energy. Smaller correlations are seen between B_l and I_{pl}, which decrease rapidly as the potential range is reduced.

5. The previous study[18] showed a very small correlation between M_d and D_{cs} or I_{pl}, which is also observed in this study for M_{13}.

3. Saddle Shape

To construct an accurate model potential surface or to obtain a good sample of a surface of any complexity, the minima, saddles, and saddle shapes of real systems need to be analyzed and the topologies characterized. To characterize the surface, we can use the "barrier ratio" (B_r) where $B_r = (B_h/B_l)$. The barrier ratio defines and thereby shows the shape of transitions, showing the relative energy gain from making a transition versus the initial cost to overcome the required barrier, providing a picture of the asymmetry of transitions that make up the surface.

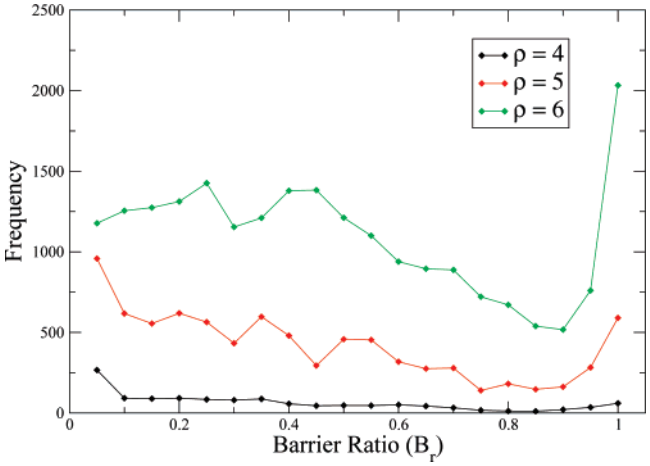

Figure 2. Frequency plot for barrier ratios (B_r) within the database of all nondegenerate transitions, for potential ranges $\rho = 4$, 5, and 6.

B_r was calculated for all transitions, and the frequency distribution was generated (using a bin size of 0.05, as shown in Figure 2.

From this figure, we draw the following observations:

1. Each potential shows an abundance of transitions with a low B_r. The number of transitions decreases as B_r increases. The higher B_r values reflect transitions with less overall gain in energy, of which there are comparitively more as the range of the potential is reduced. This observation is more obviously reflected in the mean B_r values: 0.352, 0.422, and 0.489 for $\rho = 4$, 5, and 6, respectively. The shorter-range potentials display a rougher nature, with less structure-seeking (steplike) and gradually more glass-forming (sawtooth-like) characteristics.

2. Each potential shows a large peak at $B_r \approx 1.0$, corresponding to transitions between minima of similar (or identical) energy. This peak becomes proportionally larger, compared to other B_r frequencies, as the potential range is reduced, which is partially responsible for the higher mean B_r exhibited by the shorter-range potentials.

4. Extended Disconnectivity Graphs

In this section, the standard disconnectivity graphs[16] have been extended by incorporating the integrated path length from the global minimum (I_{plgm}) as a metric for positioning basins along the x-axis.[19−21] For each minimum in the database, all monotonic sequences between that minimum and the global minimum (GM) were calculated; hence, the pathway with the shortest path length (i.e., I_{plgm}) was obtained and associated with that minimum. The minima within each superbasin at each energy level ($E_{GM} + (i \times \Delta E)$, where E_{GM} is the energy of the global minimum) were found, resulting in an I_{plgm} for each superbasin equal to the mean average of all the minima I_{plgm} values contained with that superbasin. Therefore, a disconnectivity graph shows the superbasins and their connectivity across the energy range of the database. The extended disconnectivity graphs for $\rho = 4$, 5, and 6 are shown in Figure 3. The black line shows the superbasin containing the global minimum.

The graphs show that, as the potential range is reduced, the number of superbasins increases, as do their I_{plgm} from the global minimum. The superbasins containing the GM at the highest energy shown are 4.0924, 6.6160, and 9.2987 for $\rho = 4$, 5, and 6, respectively.

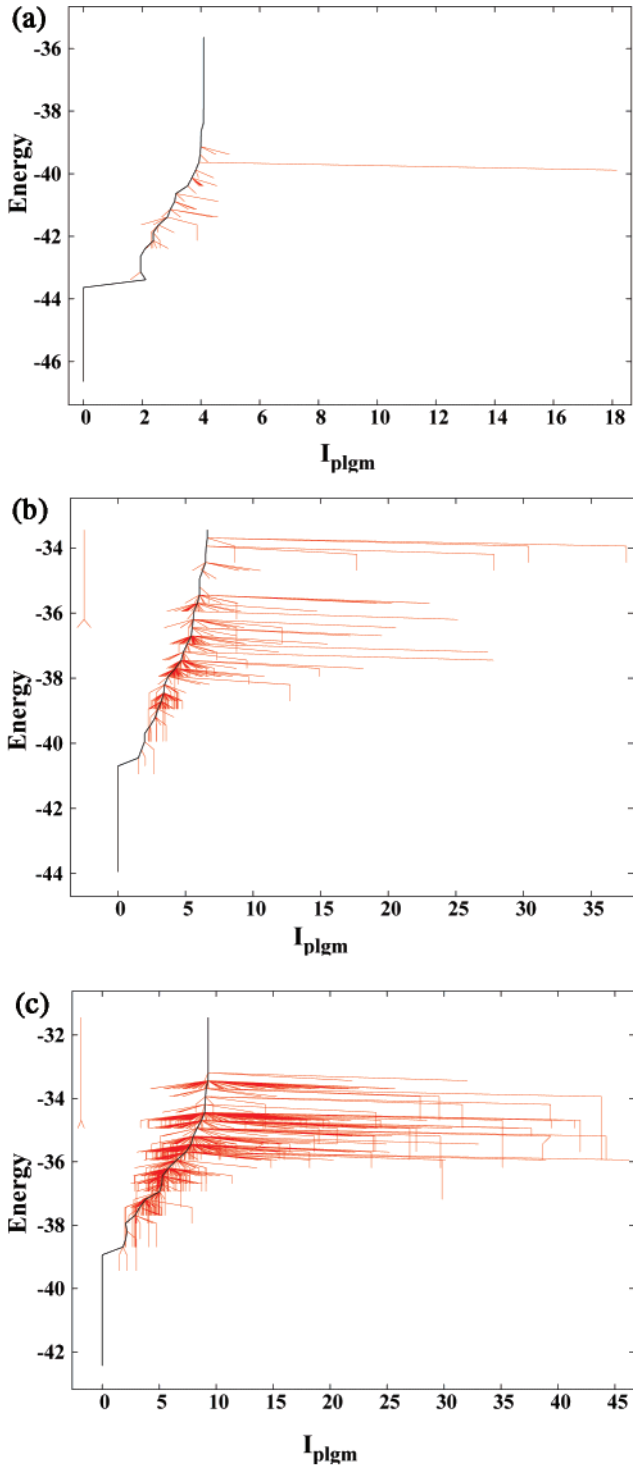

Figure 3. Disconnectivity graphs using the average integrated path length of minima from the GM (I_{plgm}) within basins to position the basins on the *x*-axis, using an energy increment of 0.25: (a) $\rho = 4$; (b) $\rho = 5$, and (c) $\rho = 6$. The basin containing the global minimum is shown in black, whereas all other basins are shown in red.

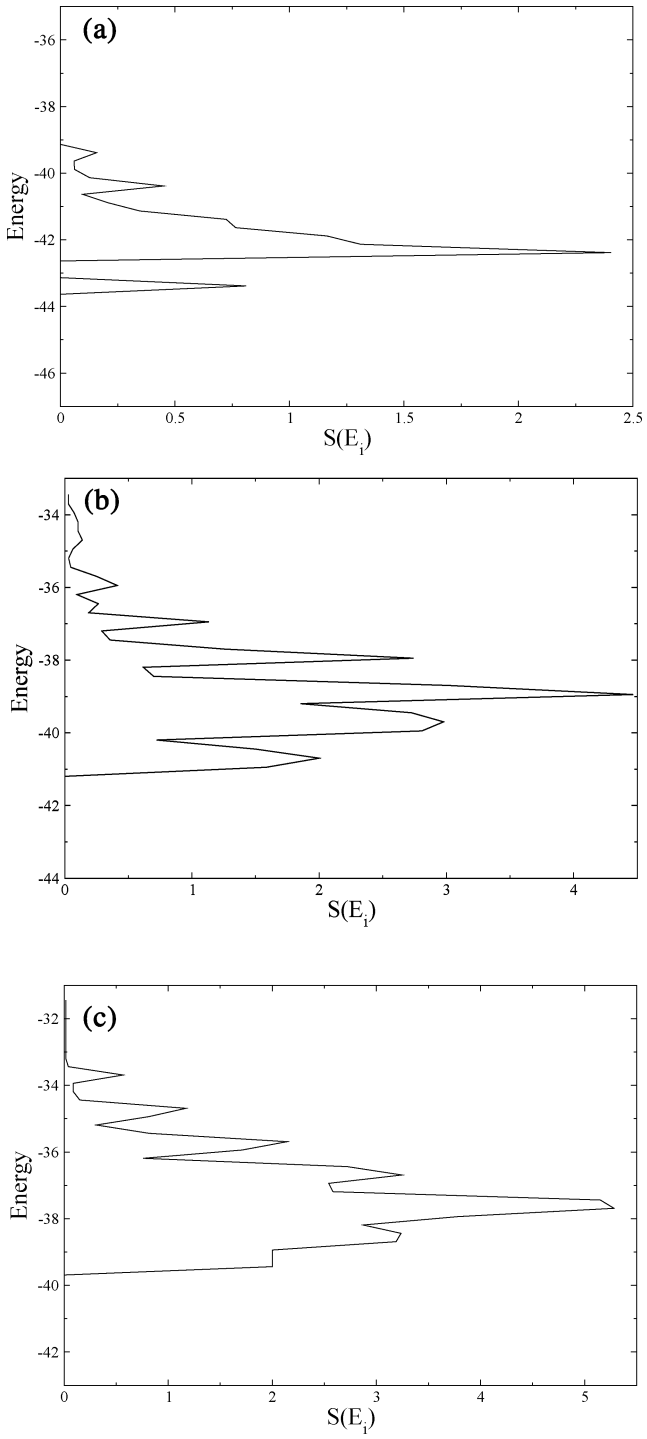

Figure 4. Distribution of Shannon entropies per energy level ($S(E_i)$) from disconnectivity graphs: (a) $\rho = 4$; (b) $\rho = 5$, and (c) $\rho = 6$.

To characterize the different potential surfaces, following the recent work of Rylance et al.[20] the complexity of the disconnectivity graphs has been calculated, using the Shannon entropy[22]

$$S(E_i) = -\sum_{x_i} P(x_i) \log_2[P(x_i)] \qquad (1)$$

where $\{x_i\}$ is the set of basins at energy $E = E_i$ and $P(x_i)$ is the probability that at E_i a variable is within a particular state/superbasin x_i. Hence, a Shannon entropy is calculated for each energy level of the disconnectivity graph. The distributions are shown in Figure 4. The higher Shannon entropies occur when there are multiple superbasins, all containing a similar number of minima.

The joint total entropy of E_i is given by

$$S_T = \sum_{i=1}^{n} S(E_i) \qquad (2)$$

where n is the number of energy levels. The normalized S_T

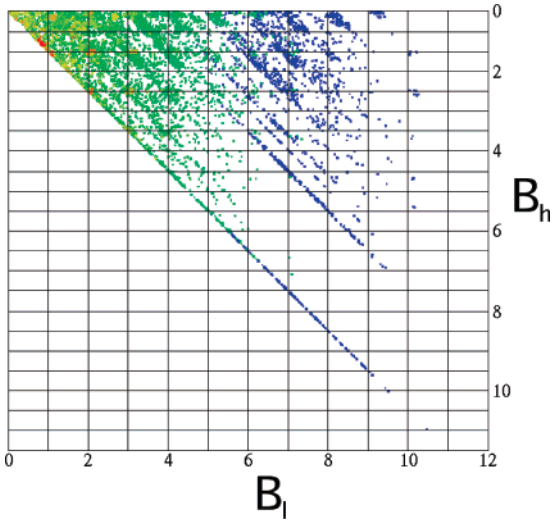

Figure 5. Bands formed for the M_{13} cluster with $\rho = 5$ by correlating the energy barrier between the lower-energy minimum and the saddle (B_l), the energy barrier between the higher-energy minimum and the saddle (B_h), and the energy of the lower-energy minimum (E_l). Colors indicate E_l values, ranging from −43.947 (blue) to −34.5785 (red).

provides a complexity measure for each disconnectivity graph, which can then be compared. The normalization involves dividing by the energy range within a database. The normalized S_T values are 0.1998, 0.7852, and 1.1507 for $\rho = 4$, 5, and 6, respectively. This indicates that the disconnectivity graphs for shorter-ranged potentials are more complex, providing a quantitative measure of the surface moving along the scale from structure-seeking toward glass-forming.

5. Barrier Heights and Energies of Minima

To extract more information about the surface and the barriers, beyond that obtained from barrier ratios, we display the distributions in three-dimensional plots of B_l vs B_h vs E_l where color provides the third dimension. As the plots for different ρ values show similar features, only the plot for $\rho = 5$ is shown in Figure 5. The scale of E_l has blue as the lowest and red the highest. Areas shown in blue refer to transitions to the lowest minimum on the surface, the global minimum (GM).

From this plot, one can observe bands of transitions, shown here as lines of transitions with the same positive gradient (1.0) and different vertical displacements. Each band corresponds to a specific M_d (i.e., $B_h = B_l - M_d$), so the intercept of each band is $-M_d$. The density of the points gives an indication of the number of transitions with similar transition measures.

There is a long band corresponding to $B_h = B_l$, that is, $M_d = 0$. As B_l increases, the density of points drops; moreover, the B_l values remain small, showing that there are many low barrier transitions leading to the global minimum.

The plots for $\rho = 4$, 5, and 6 all show the same trend discussed above, that the transitions to the GM have large B_l; however, we see a range of B_h. The database contains transitions directly connecting a large number of minima to the GM, the majority of which have low barriers, another sign from the surface topography that indicates structure-seeking behavior.

Further analysis provides a number of statistical measures, which are well-correlated with ρ and, hence, could be used to characterize the surface quantitatively. These statistics are shown in Table 2.

From Table 2, and focusing on $\rho = 5$, we see that there are 1480 transitions going to the GM via single transition states, from 459 minima. In other words, each minimum linked to the GM offers an average of about three pathways to that GM. (There are 8403 single saddle transitions and 712 minima in the database for $\rho = 5$). This gives a ratio of GM transitions/DB transitions of 0.176 and a ratio of GM-connected minima/DB minima of 0.645. The energies of the minima connected directly by single transition states to the GM span the total range of minima energies in the database (i.e., from just above the GM to −34.62, nearly the highest in the database). It can be seen that the higher the energy of E_h, the smaller the barriers for any transition: we find correlations of 0.76 for transitions involving GM and 0.61 for the whole database. This is an intuitive observation.

TABLE 2: Surface Statistics, Comparing Transitions to the GM with All Transition in the Database (DB)

statistic	$\rho = 4$	$\rho = 5$	$\rho = 6$
average GM B_h	1.544	1.670	1.657
number of GM transitions	636	1480	1824
number of DB transitions	1267	8403	21844
ratio GM/DB transitions	0.502	0.176	0.084
number of GM directly connected minima	143	459	658
number of minima in DB	160	712	1410
ratio GM/DB minima	0.894	0.645	0.467

6. Coordination and Minima Bands

Many simulations of Lennard-Jones and Morse clusters indicate that minima in the energy band just above that of the GM arise from moving a well-coordinated atom from the filled outer shell to a capping position on the cluster surface. In the case of icosahedral M_{13}, an atom can be removed from a 5-ring to a site on the surface. This process can be continued, moving highly coordinated atoms into capping positions, each time reducing the overall coordination of the structure, hence, moving the cluster to higher-energy bands of minima. This model is closely related to the "void model" for structural changes and melting of clusters.[24]

Figure 5 highlighted bands that correspond to transitions with approximately the same M_d. The band structure observed in the disconnectivity graphs and distributions in Figure 1 provides a possible explanation for the bands seen in these plots. Transitions between minima in the same band result in small differences in M_d, while transitions between minima from different bands of minima give a range of M_d.

A bond length value was obtained by calculating a pair distribution function (G_r) for interatomic distances between all pairs of minima. The maximum "bond length" was then taken as the position of the end of the first, strongest peak (4.5 Å). Therefore, any interatomic distance at or below this value represents a bond and, hence, a coordination.

The number of bonds (total coordination) in each minimum were calculated and used to calculate the change in coordination for all transitions. These values were plotted against B_l and B_h: the results for $\rho = 5$ are shown in Figure 6a.

The changes in coordination associated with a well-to-well passage range from −1 to +9 and from −2 to +9 for $\rho = 4$ and 5, respectively. Positive values refer to a gain in coordination; negative values refer to a loss. There is a clear correlation between the transition bands and the coordination change for transitions within a band. Recall that the bands correspond to different energy gaps between the two transition minima (M_d). These plots show, as expected intuitively, that the larger the difference in energy between the minima, the larger the coordination difference.

Figure 6b expands on the frequency distribution of minima energies in Figure 1 for $\rho = 5$, incorporating the coordination

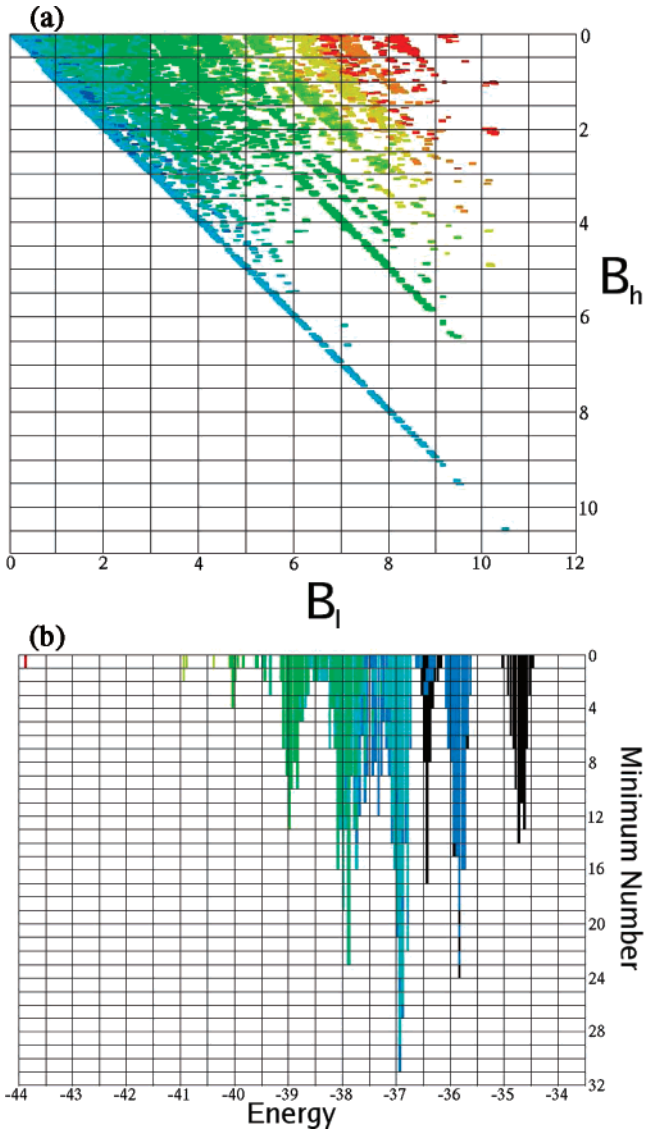

Figure 6. For the M_{13} cluster with $\rho = 5$, (a) correlation between the bands seen in the graph plotting the energy barrier between the lower-energy minimum and the saddle (B_l) vs the energy barrier between the higher-energy minimum and the saddle (B_h), and the change in coordination number, color ranging from −1 (blue) to +9 (red) (values of −2 are not visible due to the small number of points with this value); (b) frequency distribution of minima energy incorporating coordination number, color ranging from 33 (black) to 42 (red).

in each minimum by use of color. Here, black represents the lowest coordination. Although these graphs show that some minima within the same band have different coordination, this is dwarfed by the number of minima which have the same coordination. As the energies of the bands of minima increase, the coordination numbers fall. Although not completely conclusive, this provides persuasive evidence to support the aforementioned hypothesis that transitions that reduce the numbers of atom−atom contacts move the clusters to bands of minima with higher energies.

7. Band Transitions

The plots from Figures 1 and 6b, frequency distributions of energies of minima, are made up of several peaks or bands. The same is true for the distributions of the saddles; however, the overall distribution of saddles is more symmetrical. To characterize a surface sufficiently well so that one can choose a good representative sample to model kinetics accurately, we can compute the frequencies of transitions between bands of these distributions of minima and saddles, providing information about the connectivity of the surface.

TABLE 3: Band Definitions for $\rho = 5$

band number	band boundaries
1	$x > -35.5$
2	$-35.5 \geq x > -36.5$
3	$-36.5 \geq x > -37.5$
4	$-37.5 \geq x > -38.5$
5	$-38.5 \geq x > -39.5$
6	$-39.5 \geq x > -43.0$
7	$-43.0 \geq x$

The limits for the bands of minima were obtained by visual inspection, maintaining uniform band sizes. For each value of ρ, the last (lowest) band contains only the GM. The bands for $\rho = 5$ are defined in Table 3.

With the bands of minima defined, each minimum is assigned to a specific band. In this way, all transitions are scanned in the process of determining the frequency of transitions between bands. Although this analysis was carried out for $\rho = 4$, 5, and 6, only the $\rho = 5$ results are shown in Figure 7a. The colors in this graph represent the frequencies of transitions between pairs of bands.

There appears to be a shift in the bands relating to the most frequent transitions as ρ is altered. For the smoothest potential,

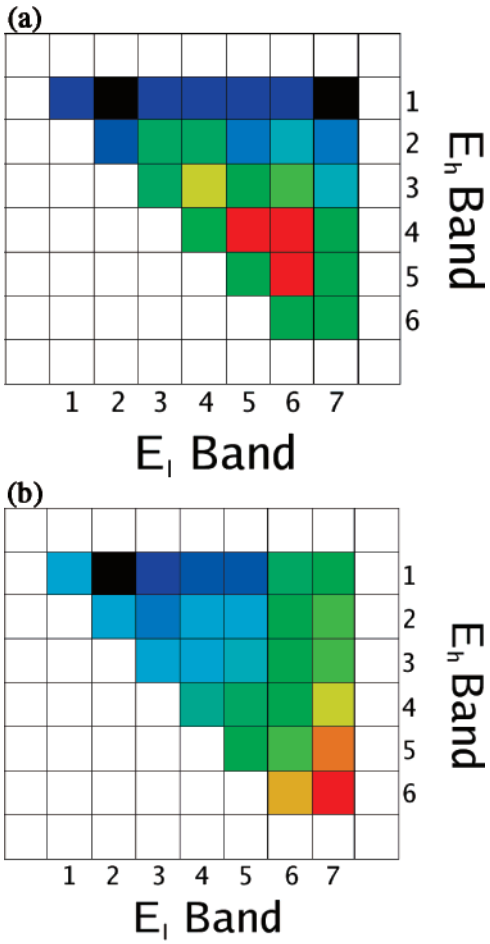

Figure 7. Frequency plot for interband transitions (i.e., between the band of minima containing the higher-energy minimum (E_h) and the band containing the lower-energy minimum (E_l)) for M_{13} clusters, $\rho = 5$: (a) absolute frequencies, color ranging from 27 (black) to 846 (red); (b) normalized frequencies, color ranging from −2.56 (black) to 1.40 (red).

TABLE 4: Number of Minima in Each Energy Band of Minima for $\rho = 4$, 5, and 6

	band number						
ρ	1	2	3	4	5	6	7
4	18	68	55	17	3	1	
5	76	149	224	187	86	15	1
6	90	381	615	278	88	13	1

with $\rho = 4$, there are many transitions from all bands to the GM band (6). The peak in the frequency of transitions to the GM occurs at band 3. For $\rho = 5$, transitions to the GM band are less frequent than those to other bands, peaking for transitions from bands 4 and 5 to band 6, one higher than the GM band. The distribution for $\rho = 6$ shows even fewer transitions to the GM band, peaking for transitions from band 3 to band 4. The graphs point toward shorter-ranged potentials having relatively fewer transitions toward and between the lowest bands of minima.

There is a large difference with band sizes, measured by their numbers of minima; as shown in Table 4, larger bands exhibit more interband transitions. The figures of transition frequency and Table 4 show that there is not a strong correlation between band size and the frequency of intraband transitions. Therefore, the graphs of transition frequencies have been normalized with respect to the number of possible transitions each band could have (N_i), as shown in eq 3. For transitions between minima in the same band (i), normalization is performed as described in eq 4, whereas normalization of transitions between different bands ($i \rightarrow i + 1$) is described in eq 5.

$$\text{freq}_N = \log_{10}\left(\frac{\text{freq}}{N}\right) \tag{3}$$

$$N = \left[\frac{N_i \times (N_i - 1)}{2}\right] \tag{4}$$

$$N = (N_i \times N_{i+1}) \tag{5}$$

All of the normalized graphs look very similar; hence, only the graph for $\rho = 5$ is shown in Figure 7b. The normalized frequencies are shown using a log scale whereby a value of zero would result if the frequency was the same as the theoretical number of possible transitions. Positive values (light green, yellow, orange, then red) show areas where there are more transitions than expected, whereas negative values (dark green and blue) show regions where there are fewer transitions than expected.

The trends observed for all values of ρ are as follows:

1. The frequency of interband transitions increases as the band of the initial state becomes lower in energy.

2. The frequency of interband transitions increases as the band of the final state becomes lower in energy.

The graphs show that multiple (minimum−saddle−minimum) pathways exist between many minima. As the bands of the initial and final minima become lower in energy, on average, the number of pathways between any two minima increases. The presence of multiple pathways can affect the overall kinetics of the system.[25]

The pattern shown by these graphs is that expected for a structure-seeker, with increasing numbers of downward transitions available as the energy drops, thereby guiding the system toward the GM. The graphs for a glass-former are expected to be significantly different, and the pattern of the bands is presumably different, because for a glass-former, most values of B_h are not very different from those of B_l, so the saddles are not very asymmetric. Moreover, for a glass-former, a large number of minima are at high energy. Hence, the graphs are expected to show a larger number of transitions between high-energy minima than for a structure-seeker, and the high values of the barrier ratio make it easy for the system to reverse any downhill steps. Hence, the glass-former's topography provides much less guidance toward any deep-lying minimum, including the GM, than does that of a structure-seeker.

The types of plots in Figure 7 could also be used to identify the presence of more than one basin in the potential energy surface. Multiple basins would correspond to multiple peaks, with the positions of the peaks depending on the energy of each of the deep basins.

7.1. Band Transition Barrier Heights. The barrier heights for transitions between two bands of minima can also be analyzed. We begin by determining the B_h distribution for transitions between any two bands. All distributions representing transitions into a given band are shown on a single graph. Each

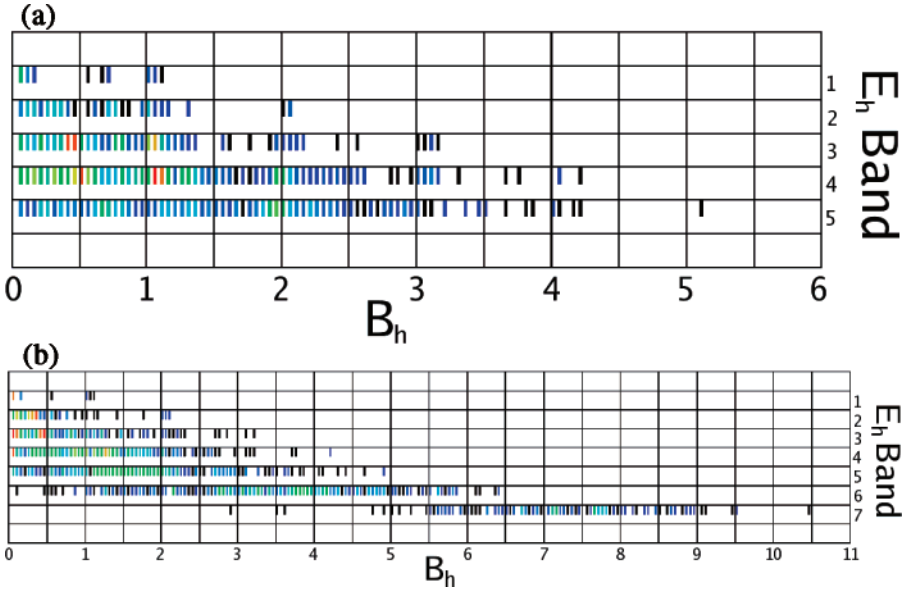

Figure 8. The barrier height between the higher-energy minimum and the saddle (B_h) distributions for band-to-band transitions for M_{13} cluster $\rho = 5$. Individual plots show the distribution of transitions from the higher-energy minima bands (E_h) into a specific lower-energy minima band (E_l): (a) $E_l = 5$; (b) $E_l = 7$.

E_l band, therefore, is represented by its own graph, Figure 8a,b. The *y*-axis of each graph indicates the index number of the E_h band from which the transitions occur. The *x*-axis shows the values of the barrier B_h, and the *z*-(color) axis shows the frequency of transitions. Figure 8 shows the results for transitions into bands 5 and 7 for $\rho = 5$.

These plots give a detailed analysis of transitions between bands of minima. In the previous section, we saw that the number of transitions between bands increases as the band energy decreases. From the present graphs, we can also see that, as the E_l energy decreases (i.e., the E_l band number increases; the GM is defined as the band with the highest index, so the other low-energy bands have high band numbers), the range of B_h values increases, with some low B_h transitions present within all possible interband transitions. Transitions from high-energy bands have the highest frequency of low barriers. There also appear to be peaks in these B_h distributions which correspond to the peaks seen in the distribution of saddle energies in Figure 1. A large number of transitions use saddles within the saddle band immediately above the minima band from which the transition occurs. Although some higher-energy saddle transitions are also possible, it is generally the low-energy pathways that are the most important in the system kinetics. (However, see ref 25 for situations that do not conform to this.)

Although the number of possible transitions between minima increases as the mean energy of the band drops, corresponding to increasing multiplicity of pathways between minima, the B_h of these transitions can vary greatly. The increasing number of transitions need not result in structure-seeking behavior of a system when the pathways are not kinetically important. It will therefore be important to perform the same analysis on a glass-former.

8. Conclusions

Through the analysis of the Morse M_{13} potentials, we find a correlation between the potential range, and hence the extent of a surface's structure-seeking behavior, and the complexity (Shannon entropy) of the extended disconnectivity graphs: complexity increases for shorter-ranged potentials. The extended disconnectivity graphs show the change in integrated path length from the global minimum (I_{plgm}) with energy. For the same energy increment, there are more superbasins for the shorter-ranged potentials, indicating larger values of barrier heights between the higher-energy minimum and the saddle (B_h).

Other correlations found are between the potential range and (i) the ratio of transitions leading toward the global minimum (GM) to the total number of transitions in the database and (ii) the ratio of minima connected to the GM to the number of minima in the database. In each case, the ratio increases for the longer-ranged, more structure-seeking potentials analyzed in this study.

The difference in coordination between minima at different energy levels has also been highlighted, supporting the hypothesis that energy bands have a useful meaning for these systems, with the bands defined by specific coordination numbers: the energy of each band is directly proportional to the number of nearest-neighbor contacts. Structural reorganizations that move highly coordinated atoms to capping positions take a system from an initial band to a higher one. This has been used to develop a general model for clusters with short-range interparticle forces.[24,26,27]

For structure-seekers, a significant number of quite asymmetric saddles, especially between bands, provides a good characterization of a model surface. A more symmetrical distribution of saddles would characterize a glass-former.

The number of transitions between different bands of minima depends on the potential. Longer-range potentials appear to yield a distribution of transitions concentrated more toward those between low-energy minima, whereas shorter-range potentials show most transitions occurring between midrange minima.

The clusters studied here are all structure-seekers, to different degrees that depend on their range. For a more quantitative analysis between structure-seekers and glass-formers, the same analysis will have to be carried out for a glass-forming cluster. For this, a study of 17 Morse particles (M_{17}), simulating Ar_{17} and related clusters, will be carried out. This system appears to have no distinct, identifiable solid−liquid phase change. In addition, an ionic cluster $(KCl)_n$, which is a structure-seeker with very long-range forces, will also be studied, for various values of *n*.

Acknowledgment. G.A.C. is grateful to the EPSRC, the School of Chemistry, University of Birmingham and the Wellcome Trust for funding. G.A.C. and R.L.J. would also like to thank G. J. Rylance (University of Birmingham) and Professor T. Komatsuzaki (Kobe University) for helpful discussions regarding disconnectivity graphs and complexity. R.S.B. wishes to thank the Aspen Center for Physics for its hospitality, when this work was being finished.

References and Notes

(1) Johnston, R. L. *Atomic and Molecular Clusters*; Taylor & Francis: London, 2002.
(2) Ball, K. D.; Berry, R. S. *J. Chem. Phys.* **1999**, *111*, 2060.
(3) Despa, F.; Berry, R. S. *J. Chem. Phys.* **2001**, *115*, 8274.
(4) Doye, J. P. K. *Phys. Rev. Lett.* **2002**, *88*, 238701−1.
(5) Wales, D. J. *Mol. Phys.* **2004**, *102*, 891.
(6) Ball, K. D.; Berry, R. S.; Kunz, R. E.; Li, F.; Proykova, A.; Wales, D. J. *Science* **1996**, *271*, 963.
(7) Kunz, R. E.; Berry, R. S. *J. Chem. Phys.* **1995**, *103*, 1904.
(8) Morse, P. M. *Phys. Rev.* **1929**, *34*, 57.
(9) Braier, P. A.; Berry, R. S.; Wales, D. J. *J. Chem. Phys.* **1990**, *93*, 8745.
(10) Wales, D. J. *Energy Landscapes*; University Press: Cambridge, 2003.
(11) Mackay, A. L. *Acta Crystallogr.* **1962**, *15*, 916.
(12) Wales, D. J.; Doye, J. P. K. *J. Chem. Soc., Faraday Trans.* **1997**, *93*, 4233.
(13) Wales, D. J. *Science* **2001**, *293*, 2068.
(14) Wales, D. J.; Doye, J. P. K. *J. Chem. Phys.* **2003**, *119*. 12409.
(15) Miller, M.; Doye, J. P. K.; Wales, D. J. *J. Chem. Phys.* **1999**, *110*, 328.
(16) Despa, F.; Wales, D. J.; Berry, R. S. *J. Chem. Phys.* **2005**, *122*, 024103−1.
(17) Berry, R. S.; Elmaci, N.; Rose, J. P.; Vekhter, B. *Proc. Natl. Acad. Sci. U.S.A.* **1997**, *94*, 9520.
(18) Wales, D. J. *J. Chem. Phys.* **1994**, *101*, 3750.
(19) Komatsuzaki, T.; Hoshino, K.; Matsunaga, Y.; Rylance, G. J.; Johnston, R. L.; Wales, D. J. *J. Chem. Phys.* **2005**, *122*, 084714.
(20) Rylance, G. J.; Johnston, R. L.; Matsunaga, Y.; Li, C. B.; Baba, A.; Komatsuzaki, T. Manuscript in preparation.
(21) Cox, G.; Johnston, R. L. *J. Chem. Phys.*, in press.
(22) Shannon, C. E. *Bell Syst. Tech. J.* **1948**, *27*, 379−423 and 623−656.
(23) Trygubenko, S. A.; Wales, D. J. *J. Chem. Phys.* **2004**, *121*, 6689.
(24) Berry, R. S.; Smirnov, B. M. *Phys. Usp.* **2005**, *48*, 345.
(25) Zaman, M. H.; Sosnick, T. R.; Berry, R. S. *Phys. Chem. Chem. Phys.* **2003**, *5*, 2589.
(26) Berry, R. S.; Smirnov, B. M. *JETP* **2003**, *93*, 541.
(27) Berry, R. S.; Smirnov, B. M. *JETP* **2004**, *98*, 366.